Silicon (2021) 13:857–865
https://doi.org/10.1007/s12633-020-00485-3

ORIGINAL PAPER

New Nano-Bioactive Glass/Magnesium Phosphate Composites by Sol-Gel Route for Bone Defect Treatment

M. M. Farag[1] · H. H. Liu[2] · A.H. Makhlouf[3]

Received: 12 January 2020 / Accepted: 13 April 2020 / Published online: 17 May 2020

Abstract

This work was mainly aimed to synthesize new ceramic composites based on nano-bioactive glass (nBG) and magnesium phosphate ceramic (MgP) with different ratios using the sol-gel approach in order to overcome the limitations of both materials. The glass was based on $85SiO_2$-$10CaO$-$5P_2O_5$ (mole %), and MgP was based on the formula; $Mg_3(PO_4)_2$. The obtained composites were characterized by DTA, XRD, FTIR, SEM/EDX and Zeta potential techniques. The in vitro bioactivity test was carried out in SBF, and the cell viability test was conducted by culturing the composites with human normal fibroblast cell line (BJ1). The results of XRD analyses showed that there were often no strong diffraction peaks detected which indicated the amorphous nature of the ceramic composites. Moreover, soaking of the ceramic composites in SBF exhibited that addition of MgP to nBG was increased the degradation of the latter one, and nBG was improved the formation of apatite crystals on MgP ceramic. Moreover, the cell viability results showed that MgP was showed significant higher viability than nBG at high concentrations, and it improved the viability of nBG in the ceramic composites.

Keywords Nano-bioactive glass · Mg-phosphate · Composite · Sol-gel

1 Introduction

The bone defects caused by accidents, bone tumor or aging rank second in the surgeries that require tissue transplantation annually in the USA [1]. Although the autografting is the best solution for treatment of bone defect, this method still has some shortage, such as unavailability of bone tissue in most cases and it requires additional surgery which causes more pain for the patient [2]. Accordingly, the research and development of new synthetic bone substitutes exhibiting properties similar or even close to the natural bone is still a challenge in the orthopedic research [3, 4]. There have been several synthetic materials used as bone substitutes, such as calcium phosphates (CaPs), including hydroxyapatite and tricalcium phosphate [5], magnesium phosphates (MgPs) [6, 7] and bioactive glasses (BGs) [8].

Whereas CaPs are osteoconductive materials, their surface reactivity and solubility are relatively low [5, 9]. MgPs have been drawing more attention in the recent years as alternative materials for CaPs in the biomedical applications. Where, they are biocompatible [6, 7], and their cements are characterized by high mechanical strength comparable to other bone substitutes, such as brushite [10], as well as, they have biodegradability and surface reactivity higher than most derivatives of CaPs [10, 11]. Moreover, MgP minerals are proven to be biocompatible with bone-forming cells [12]. Generally, Mg element stimulates new bone formation and increases bone cell adhesion and stability [13, 14]. However, like CaPs, the osteoconductivity of MgPs is not enough to accomplish a bone defect filling under acute conditions, such as old patients with metabolic illnesses and sites of poor vascularization. And so, introducing of osteoinductive materials into MgPs, such as bioactive glasses (BGs) is crucial to enhance their bioactivity function.

In the last decades, BGs have been used widely as bone substitutes due to their osteostinductivity and their ability to

✉ M. M. Farag
mmfaragnrc@gmail.com

[1] Glass Research Department, National Research Centre, 33 El Bohouth Str., Dokki, Giza 12622, Egypt

[2] Department of Bioengineering, MSE227 Materials Science and Engineering Building, University of California, Riverside, Riverside, CA 92521, USA

[3] Manufacturing Engineering Department, College of Engineering and Computer Science, University of Texas Pan-American, Edinburg, TX 78539-2999, USA

form a chemical bond with the surrounding tissues throughout a formation of hydroxyapatite layer at the glass/tissue interface [15, 16]. Moreover, the properties of BGs can be tailored by changing their compositions, and their angiogenic and osteogenic effects on the cells depend on the ions released from them [17, 18]. Mostly, BGs were synthesized by conventional melting of oxides. The discovery of sol-gel chemistry in 1991has been given rise to a new generation of bioactive glasses [19]. One of the most attractive characteristics of the sol–gel method is allowing researchers to obtain nano-systems based on sol-gel bioactive glass as nanoparticles and nanofibers, which are promising candidates in biomedical applications [20]. However, the biodegradation rates of BGs are usually slow compared to some kinds of bioresorbable ceramics (such as, tricalcium phosphate and brushite). That is because of formation of new insoluble apatite crystals in the biological fluids. Therefore, addition of highly degradable ceramics, such as MgP ceramic, to BG will increase the degradation rate of BG by suppressing or even decrease the formation of these insoluble apatite crystals [21].

The main aim of this work is the enhancement of the bioactivity of MgP ceramic by introducing nano-bioactive glass (nBG), as well as, the increase of degradation of nBG by MgP. This was carried out by preparing new nBG/MgP composites using sol-gel method to combine the advantages of both components. The published research addresses this type of composites is very scarce, and this study is the first one concerning with synthesis of this kind of composites which are expected to be promising materials for the bone defect treatment.

2 Materials and Methods

2.1 Preparation of mg-Phosphate (MgP) Ceramic

The suggested MgP ceramic in this work was based on farringtonite mineral formula, $Mg_3(PO_4)_2$. Where, it was prepared by the reaction of $MgCO_3$ and H_3PO_4. The solution of 0.67 M of H_3PO_4 was added dropwise on 1 M of $MgCO_3$ solution, and the mixture was stirred for 10 h and left 24 h for aging. And the precipitate was filtered and dried at 80 °C for 2 days and used as it is in the synthesis of nBG/MgP composites thereafter.

2.2 Preparation of nBG/MgP Composites

The glass composition based on $85SiO_2$-$10CaO$-$5P_2O_5$ was prepared by the quick alkali-mediated sol-gel method. TEOS (tetraethyl orthosilicate), $Ca(NO_3)_2{\cdot}4H_2O$, TEP (triyethyl phosphate), ethanol (EtOH), nitric acid (HNO_3) and ammonia chemicals with analytical grade were used as received to synthesize these materials. In a typical synthesis of nBG, TEOS was added to a mixture of 2 M HNO_3 and ethanol solution with a molar ratio TEOS: EtOH: H_2O = 1:8:10. After complete hydrolysis of TEOS, TEP and $Ca(NO_3)_2{\cdot}4H_2O$ were added to the solution, respectively, with 30 min time interval, and the solution left to stir for 4 h. And then, different weight percentages (0, 25, 50 and 100 wt.%) of previously prepared MgP powder were added (the samples accordingly encoded G, MP25, MP50 and MP, respectively, Table 1) and stirred for 2 h. Ammonia solution was added to the mixture solution with vigorous stirring. As a result, the transparent sol was quickly changed to opaque white gel, and thoroughly, this gel was stirred mechanically to hider an aggregation of the gel. Thereafter, the obtained gel was dried at 50 °C in the oven for 2 days to remove the residual water and ethanol. Finally, the dry gel powders were calcined at 600 °C (with heating rate 5 °C/min) in air for 30 min.

2.3 Characterization of nBG/MgP Composites

The obtained composites were characterized by differential thermal analysis (DTA) using Setaram, heating from 25 to 700 °C at a rate of 40 °C.min^{-1} to determine the thermal behavior of the as-prepared gels. The particle size and the morphology of the composite powders were investigated by scanning electron microscope (SEM), model Hitatchi S-5500, in which a very minute amount of powder was directly mounted on the carbon tap and then coated with gold to be examined by SEM. The formed crystalline phases were detected by x-ray diffraction (XRD) using a Philips PW1390 X-ray diffractometer (U.S.D.) at room temperature in the 2θ range from 10 to 70° in 0.02° steps using CuKα radiation (1.5418 Å). Moreover, the characteristic vibration modes were determined by Fourier transform infrared (FTIR) technique at room temperature in the wavenumber range of 4000–400 cm^{-1} using JASCO FT/IR-4600 by mixing 2 mg of the sample powder with 200 mg KBr in an agate mortar and pressed into a pellet. Zeta potential of the composite ceramics was measured by Zetasizer NanoZS, Malvern Panalytical, UK, in the double distilled water.

2.4 In Vitro Degradation Test

The in vitro biodegradation test was evaluated in the simulated body fluid (SBF) at pH 7.4 prepared according to Kokubo and Takadama [22]. The ceramic samples were shaped in discs by compressing 0.2 g of powder uniaxially in stainless steel mold with diameter of 8 mm using pressure of 2 MPa. The ceramic composite discs were immersed in the high density polyethylene (HDPE) bottles contained SBF solution. The soaking solution was wholly collected and replaced by fresh SBF at predetermined times (1, 3, 7, 14 and 21 days), and Ca, P and Mg ions concentrations released from the samples into the solutions were measured colorimetricaly using BIODIGNOSTIC kits, Egypt, as well as, the change of pH

Table 1 The composite compositions based on the ratios between nBG and MgP in wt.%, the endothermic and exothermic temperatures (°C) of DTA analysis, Zeta potential (mV), and Ca/P ratio of samples after immersion in SBF

Sample	Composite composition (wt.%)		DTA temperatures (°C)		Zeta potential (mV)	Ca/P
	nBG	MgP	Endo	Exo		
G	100	0	98	277	−16.1	2.56
MP25	75	25	114	271	−14.9	0.84
MP50	50	50	137	281	−13.1	1.36
MP	0	100	205	–	−11.1	–

of the solution with the time followed up. In addition, the weight loss % of the samples was measured and calculated depending on the following equation.

$$\text{Wt.loss\%} = (\text{Wi}-\text{Wd}/\text{Wi})*100$$

Where, Wi and Wd are the initial weight and dried weight, respectively, after immersion. Moreover, the change of samples surfaces after immersion in the solution was investigated by scanning electron microscope coupled with energy dispersive X-ray analysis; Model, Hitachi SU8000 attached with EDX Unit (Thermoscientific), with accelerating voltage 30 KV, magnification up to 100,000x.

2.5 Cell Viability Test

The cell viability of the prepared composites was studied using human normal fibroblast cell line (BJ1) using MTT (3-(4,5-dimethylthiazol-2-yl)-2,5-diphenyl tetrazolium bromide) [23]. The cell solution was prepared by suspending the cells in DMEM-F12 medium contained 25 µg/ml amphotericin B, 10,000 µg/ml streptomycin sulfate, 10,000 U/ml potassium penicillin and 1% L-glutamine at 37 °C under 5% CO_2 using a water jacketed CO_2 incubator (Sheldon, TC2323, Cornelius, OR, USA). After culturing of the cells for 5 d, the cells of concentration equal 1×10^3 were seeded on different concentrations of ceramics (125, 500, 1000 and 2000 µg/ml) at 37 °C for 24 h under 5% CO_2 in 96-well plates. Fresh medium without cells was used as a negative control, and another one with cells was used as a positive control under the same conditions, and then, the absorbance was measured using the microplate multi-well reader (Bio-Rad Laboratories Inc., model 3350, USA) at 595 nm. The viable cells percentage was calculated by the following equation:

$$(\text{ODt}/\text{ODc}) \times 100\%$$

Where ODt and ODc are the mean optical density of the wells treated with the sample and the mean optical density of the untreated cells, respectively.

2.5.1 Statistical Analysis

The experimental data obtained in this study were expressed as the average ± standard deviation (SD) for $n = 3$ and were analyzed using standard analysis of Student's t test. The level of significance (p value) was set at <0.05.

3 Results and Discussion

3.1 Characterization of nBG/MgP Composite

3.1.1 DTA

The thermal decomposition of the as-prepared dried gels was investigated by DTA. Table 1 and Fig. 1 show the endothermic and exothermic peaks of G, MP25, MP50 and MP. As shown in the figure, there were broad and weak endothermic peaks at 98 °C, 114 °C and 137 °C for G, MP25 and MP50, respectively, which referred to the evaporation of adsorbed water. Whereas, very strong and sharp peak was observed at 205 °C for MP sample which likely assigned to removal of

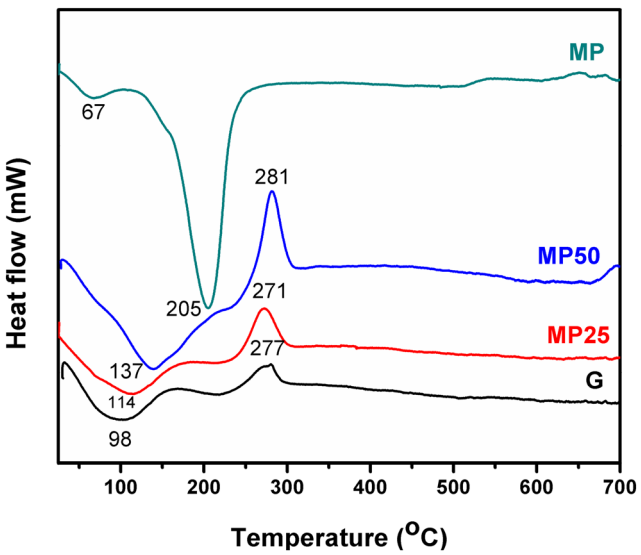

Fig. 1 DTA traces of G, MP25, MP50 and MP samples

physically adsorbed water and water molecules presented in the building structure of MgP. The exothermic peaks were noticed at 277 °C, 271 °C and 281 °C for G, MP25 and MP50, respectively, which ascribed to the loss of organics components of the precursors (i.e. alkyl groups in TEOS). According to the DTA curves, the temperature selected for sintering of the composite samples was 600 °C to avoid crystallization of them.

3.1.2 Particle Size and Morphology by SEM

The particle size and shape of different composites were examined using SEM (Fig. 2). Very minute amount of the sample powder was mounted on the carbon tap and coated with gold thereafter. As shown from the figure, the particle shape of nBG was spherical and the size was less than 100 nm. Addition of MgP to the glass was increased the aspect ratio of the grains and formed fibrous composite particles (Fig. 2b, c for MP25 and MP50, respectively). The grain shape of MP sample was anhedral, and the boundaries between the particles were unclear.

3.1.3 XRD Analysis

Figure 3 represents XRD analysis of G, MP25, MP50 and MP samples. From the figure it can be noted that there was no diffraction pattern detected in XRD spectrum of sample G which indicated the amorphous structure of glass sample. Whereas, weak diffraction peaks were detected in the composite samples (MP25 and MP50), the peaks were attributed to the formation of magnesium phosphate phase, $Mg_2P_4O_{12}$ (PDF# 00-040-0067). In contrast, very weak diffraction peaks of $Mg_2P_2O_7$ crystals were observed for MP sample (PDF # 00–008-0038).

3.1.4 FTIR Analysis

The vibration modes of the characteristic groups in different nBG/MgP composites were investigated by FTIR analysis. Figure 4 shows FTIR spectra of G, MP25, MP50 and MP samples. As shown from the figure, the spectrum of nBG (sample G) shows Si-O-Si bending vibration modes at 466 cm^{-1}, and the P-O bending mode was detected at 464 cm^{-1}. Moreover, the bending vibration mode of O-Si-O of orthosilicate SiO_4^{4-} and Si-O-Si asymmetric stretching vibration was observed at 800 cm^{-1} and 1099 cm^{-1}, respectively. The shoulder remarked at about1218 cm^{-1} was attributed to Si-O-Si bending mode. The FTIR spectrum of pure Mg phosphate (sample MP) demonstrated strong absorption band in 900–1300 cm^{-1} range due to P-O stretching vibration modes of pyrophosphate. The absorption bands at 1066 and 944 cm^{-1} were ascribed to P-O stretching vibrations of crystalline $PO^{3-}{}_4$ groups. There were additional bands at 777, 650, and 574 cm^{-1} which can be attributed to P-O-P vibrations. Addition of MgP to the glass (samples MP25 and MP50) was caused a shift of Si-O-Si asymmetric stretching vibration to higher frequency.

3.1.5 Zeta Potential

The Zeta potential values of G, MP25, MP50 and MP samples are shown in Table 1. All samples demonstrated negative values of Zeta potential in the double distilled water; they were − 16.1 mV, −14.9 mV, −13.1 mV and − 11.1 mV for G, MP25, MP50 and MP, respectively. As noticed from these

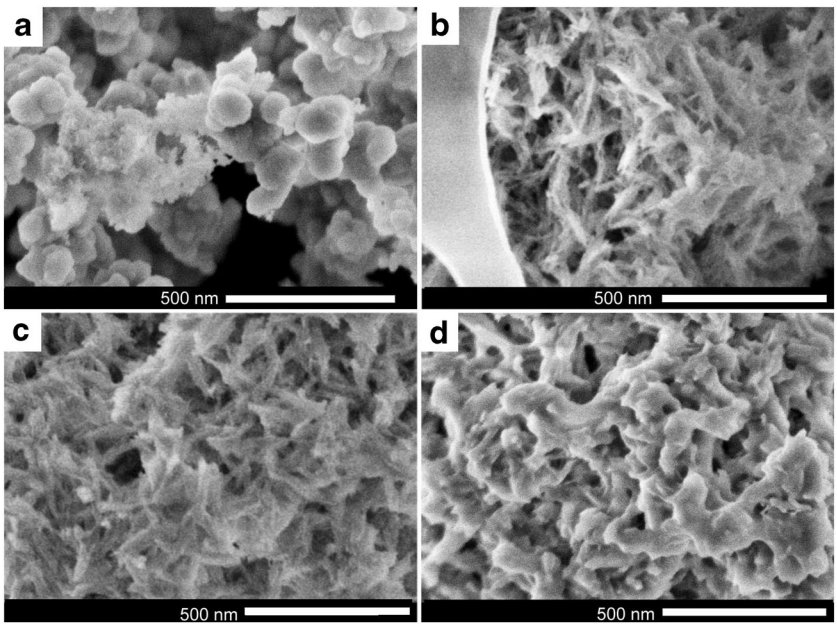

Fig. 2 SEM of G, MP25, MP50 and MP samples (**a**, **b**, **c** and **d**, respectively)

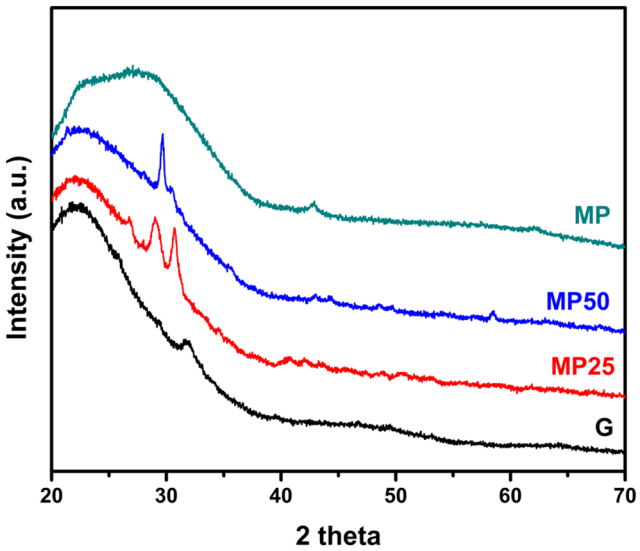

Fig. 3 XRD spectra of G, MP25, MP50 and MP samples

results, the surface charges of the prepared samples were shifted to more negative value as the percentage of nBG increased. And consequently, addition of nBG to MgP was showed an advantage to increase the electronegative surface charge of MgP ceramic. According to previous studies, the material surface of more negative Zeta potential is more favourable to attach and proliferate osteoblast cells than that of less negative Zeta potential [24–27]. However, as it will be shown in this study (in the cell viability section), the viability findings were more dependent on the ceramic composition than its charge because of the charge differences between different composite ceramics were relatively small.

3.2 In Vitro Bioactivity and Degradation Test

A widely used non-cellular method to determine the capability of materials to bond to living bone tissue is its possibility to form a bone-like apatite layer on their surface after immersion in SBF. This bone-like apatite layer provides the capability of materials surface to form direct contact with human bone living cells. Figure 5 shows the SEM and EDX analysis of the surface of G, MP25, MP50 and MP samples after immersion in SBF for 21 days. After SBF immersion, SEM micrographs showed an aggregation of spherical particles on G, MP25 and MP5 sample surfaces. The corresponding EDX spectrum of the newly formed surface layer showed high concentrations of Ca and P in comparison to Si for both samples. The calculation of Ca/P molar ratios from EDX analysis showed that G sample (nBG) was showed the highest value (2.56), while MP25 showed the lowest one (0.84). Comparatively, the Ca/P ratio of MP50 (1.36) was the nearest ratio to the stoichiometric HAp (1.67) among other samples. However, there was no peak for Ca detected in EDX analysis the surface of MP sample, which referred to an absence of new hydroxyapatite (HAp) crystals. Previous studies were reported that HAp crystals can be formed on the surface of Mg phosphate ceramics after immersion in SBF [28, 29], but, the results obtained in this study were contrary to these previous results.

The change of pH of G, MP25, MP50 and MP was investigated by measuring pH values of incubated SBF at predetermined times. Figure 6a shows the variation of pH with the time after immersing in SBF up to 21 days. It can be noted from the figure that the pH values were decreased during the first week of immersion to 7.26, 7.37 and 7.38 for G, MP25 and MP50, respectively. This was likely due to a rapid ion exchange between Ca^{2+} and H^+ or H_3O^+ in SBF solution which caused an increase of hydroxyl groups in the solution. As a result of this process, Si-O-Si glass network bonds were broke down and silica-rich layer composed mainly of SiOH (silanol) groups was formed on the glass surfaces. The newly formed silanol layer has the affinity to attract Ca^{2+} and PO_4^{3-} from the surrounding solution to form amorphous Ca-phosphate layer which crystalizes to bone-like apatite crystals in the later stage. pH values were almost constant during the rest of immersion time as a result of a formation of the protective apatite layer on the glass surface. In contrary, pH increased again for MP sample after decrease stage during the first week. This can be attributed to release of Mg-OH species from the ceramic surface.

The weight loss percentage of different samples was measured as a function of time (Fig. 6b). It was noted that addition of MgP ceramic to nBG was increased the degradation of the resulted composites. That was due to a higher degradation of MgP ceramic than nBG. Accordingly, the degradation of such composites can be tailored by changing of MgP ratio in the samples.

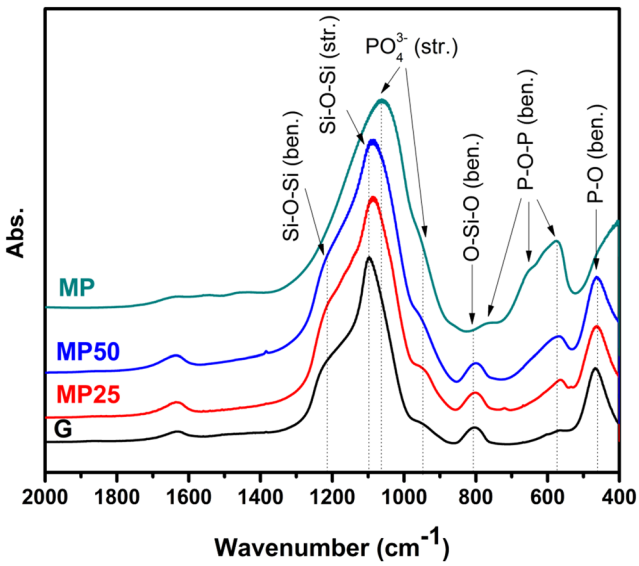

Fig. 4 FTIR spectra of G, MP25, MP50 and MP samples

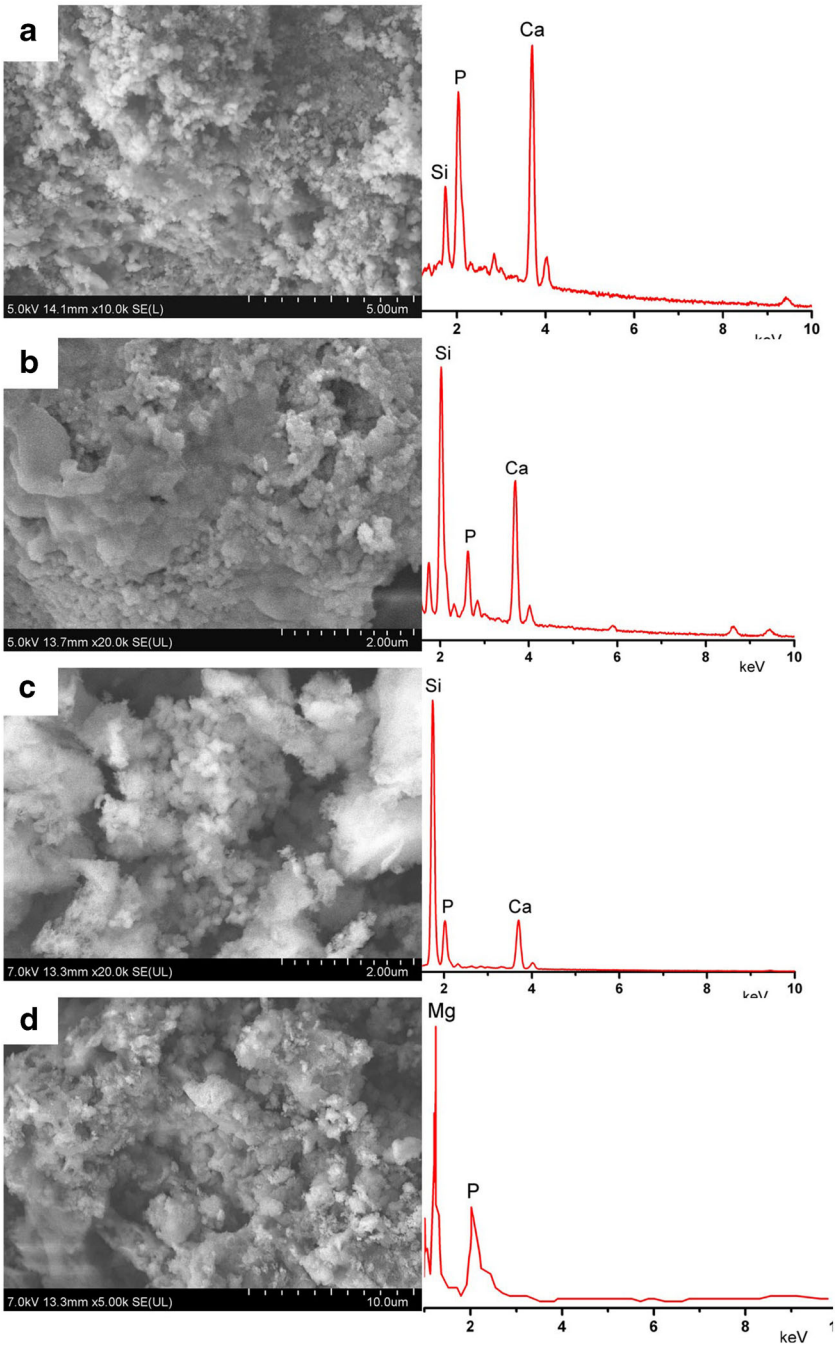

Fig. 5 The cell viability (%) of G, MP25, MP50 and MP samples after 24 h treatment against BJ1 (human normal skin fibroblast) cell line using MTT assay

The change of concentrations of Mg, P and Ca ions in SBF were also investigated as a mark of hydroxyapatite formation on the glass surfaces. Figure 6c-e shows the concentration of Mg, P and Ca ions in SBF solution incubated G, MP25, MP50 and MP samples. The concentration of Mg ions released into the solution was almost constant for MP25, MP50 and MP samples, this was because of release of Mg ions from MgP ceramic beside the initial concentration of Mg ions in SBF. The concentration of P ions released from G sample was increased during the first week of immersion and followed by almost constant value. That was due to formation of apatite layer on the glass surface. In contrast, the concentrations reached to maxima at 3, 14 and 7 d for MP25, MP50 and MP, respectively, followed by a decrease in concentrations. This can be explained by the dissolution of phosphate ions from MgP ceramic and reprecipitation of these phosphate ions as new species of Mg phosphates. The concentrations of Ca^{2+} ions in SBF incubated different samples were decreased during 3 d of incubation and followed by nearly constant values till the end of immersion time. This was due to a depletion of Ca^{2+} ions in the formation of calcium phosphate crystals in case of the fluid incubated G, MP25, and MP50 samples.

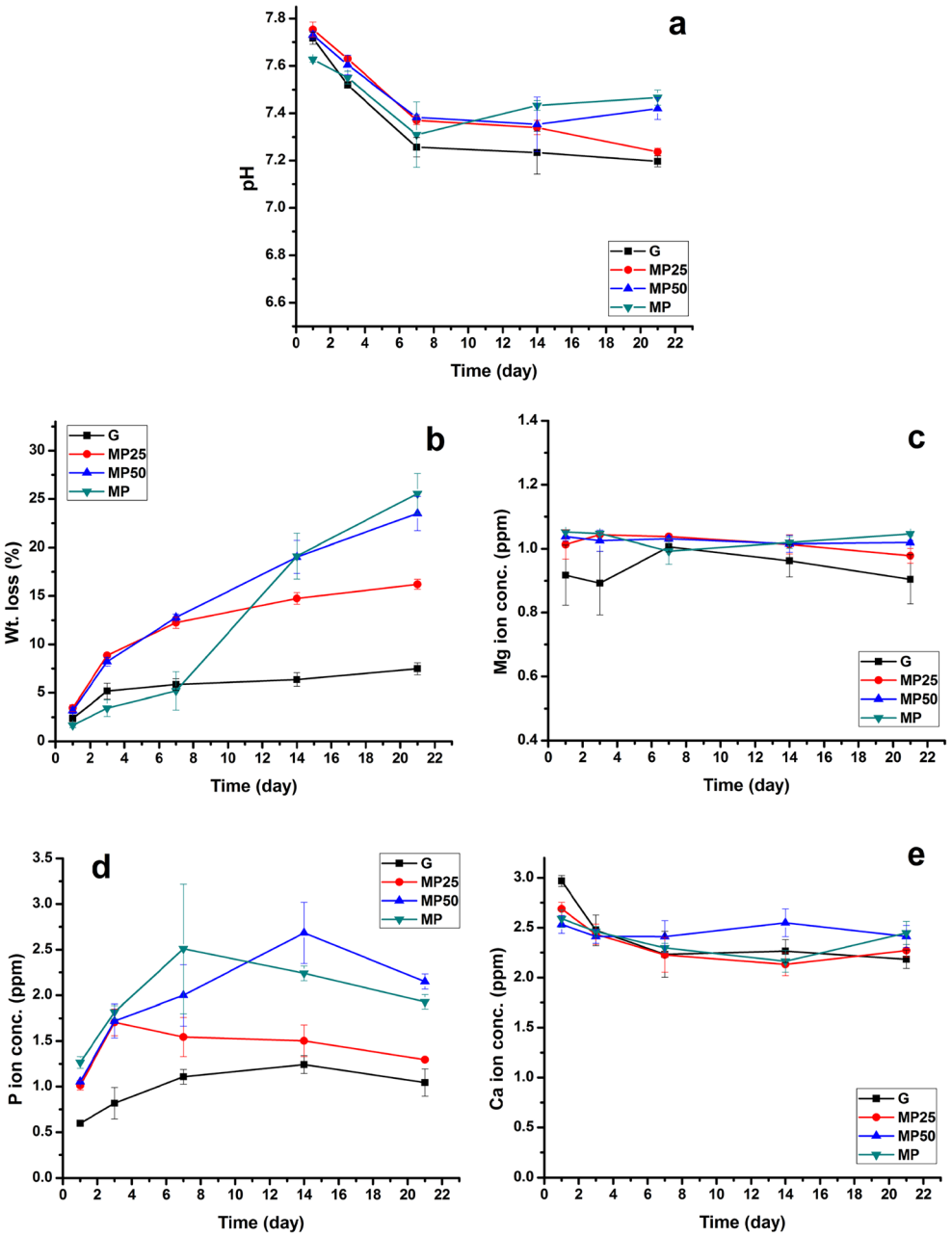

Fig. 6 pH (**a**), wt. loss % (**b**), Mg ion concentration (**c**), P ion concentration (**d**) and Ca ion concentration (**e**) of G, MP25, MP50 and MP after immersion in SBF for 21 d

3.3 Cell Viability

In order to study the cytotoxicity of different ceramic composites, different concentrations of the composite powders (125, 500, 1000 and 2000 μg/ml) were cultured on human normal fibroblast cell line (BJ1) for 24 h using MTT assay (Fig. 7). The cell viability results obtained in this study for nBG (G sample) were similar to that we obtained previously for other bioactive glass nanoparticles against human lung fibroblast normal cell line (WI-38 cells) [30]. Moreover, the results exhibited that MP sample was had a significant ($p < 0.05$) higher cell viability than other composites at all concentrations, except at concentration 125 μg/ml, there was no significant difference ($p > 0.05$) between G and MP samples. Addition of MgP to nBG was significantly improved the viability of the latter one, specifically at concentrations 500 and 1000 μg/ml. Higher cell viability of MP than G can be attributed to lower degradation of nBG (sample G) than MgP (sample MP). This a relatively high degradation of MgP ceramic caused enrichment of the cell medium with Mg^{2+} ions which improved the cell growth conditions as reported before [31]. However, the surface charge of ceramic powders did not likely demonstrate an obvious effect on the cytotoxicity results, that was due to the charge differences between the composite ceramics were small (Zeta potential = 16.1 mV, −14.9 mV, −13.1 mV and − 11.1 mV for G, MP25, MP50 and MP).

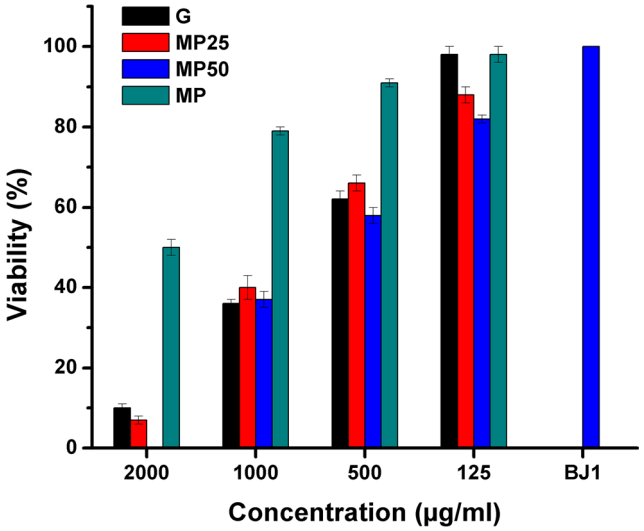

Fig. 7 The cell viability (%) of G, MP25, MP50 and MP samples after 24 h treatment against BJ1 (human normal skin fibroblast) cell line using MTT assay

Therefore, the cell viability results were more dependent on the ceramic composition than its charge.

4 Conclusion

In the present study new nBG/MgP composites were prepared successfully in order to overcome the limitations of nBG and MgP. The weak diffraction peaks of $Mg_2P_4O_{12}$ crystals were detected by XRD in the composites (MP25 and MP50), while, no diffraction peaks were detected for nBG and MgP. The Zeta potential results showed that addition of nBG to MgP was increased the negative charge of the latter one. Moreover, the in vitro bioactivity test of the ceramic composites in SBF demonstrated that the addition of MgP to nBG was increased the degradation of nBG, and in parallel nBG was improved the formation of bone-like apatite crystals on MgP ceramic particles. Moreover, the cell viability results showed that MgP was showed significant higher viability than nBG at high concentrations due to the release of Mg^{2+} ions from MgP ceramic which improved the cell growth conditions, and the results showed that the cytotoxicity was more dependent on the ceramic composition than its charge.

Acknowledgements This work was funded by Science and Technology Development Fund (STDF) under the project no. 24217. The authors would like to thank the National Research Centre (Biomaterials Group) and University of California Riverside, USA, for a possibility to use their facilities.

Compliance with Ethical Standards

Conflict of Interest The authors declare that there have no conflicts of interest.

References

1. Wang W, Yeung KW (2017) Bone grafts and biomaterials substitutes for bone defect repair: a review. Bioactive materials 2(4):224–247
2. Dimitriou R, Mataliotakis GI, Angoules AG, Kanakaris NK, Giannoudis PV (2011) Complications following autologous bone graft harvesting from the iliac crest and using the RIA: a systematic review. Injury 42:S3–S15
3. Giannoudis PV, Dinopoulos H, Tsiridis E (2005) Bone substitutes: an update. Injury 36(3):S20–S27
4. Zimmermann G, Moghaddam A (2011) Allograft bone matrix versus synthetic bone graft substitutes. Injury 42:S16–S21
5. LeGeros RZ (2008) Calcium phosphate-based osteoinductive materials. Chem Rev 108(11):4742–4753
6. Jongman Lee MMF (2014) Eui Kyun Park, Jiwon Lim, Hui-suk Yun, *A simultaneous process of 3D magnesiumphosphate scaffold fabrication and bioactive substance loading for hard tissue regeneration*. Mater Sci Eng C 36:52–260
7. M.M. Farag, H.-s.Y., Effect of gelatin addition on fabrication of magnesium phosphate-based scaffolds prepared by additive manufacturing system. Mater Lett, 2014. 132: p. 111–111, 115
8. Hench LL, Jones JR (2015) Bioactive glasses: frontiers and challenges. Frontiers in bioengineering and biotechnology 3:194
9. Bellucci D, Sola A, Anesi A, Salvatori R, Chiarini L, Cannillo V (2015) Bioactive glass/hydroxyapatite composites: mechanical properties and biological evaluation. Mater Sci Eng C 51:196–205
10. Moseke C, Saratsis V, Gbureck U (2011) Injectability and mechanical properties of magnesium phosphate cements. J Mater Sci Mater Med 22(12):2591–2598
11. Yu Y, Wang J, Liu C, Zhang B, Chen H, Guo H, Zhong G, Qu W, Jiang S, Huang H (2010) Evaluation of inherent toxicology and biocompatibility of magnesium phosphate bone cement. Colloids Surf B: Biointerfaces 76(2):496–504
12. Tamimi F, Nihouannen DL, Bassett DC, Ibasco S, Gbureck U, Knowles J, Wright A, Flynn A, Komarova SV, Barralet JE (2011) Biocompatibility of magnesium phosphate minerals and their stability under physiological conditions. Acta Biomater 7(6):2678–2685
13. Zreiqat H, Howlett CR, Zannettino A, Evans P, Schulze-Tanzil G, Knabe C, Shakibaei M (2002) Mechanisms of magnesium-stimulated adhesion of osteoblastic cells to commonly used orthopaedic implants. Journal of Biomedical Materials Research: An Official Journal of The Society for Biomaterials, The Japanese Society for Biomaterials, and The Australian Society for Biomaterials and the Korean Society for Biomaterials 62(2):175–184
14. Yamasaki Y, Yoshida Y, Okazaki M, Shimazu A, Uchida T, Kubo T, Akagawa Y, Hamada Y, Takahashi J, Matsuura N (2002) Synthesis of functionally graded MgCO3 apatite accelerating osteoblast adhesion. Journal of Biomedical Materials Research: An Official Journal of The Society for Biomaterials, The Japanese Society for Biomaterials, and The Australian Society for Biomaterials and the Korean Society for Biomaterials 62(1):99–105
15. Cao W, Hench LL (1996) Bioactive materials. Ceram Int 22(6):493–507
16. Hench LL, Splinter RJ, Allen WC, Greenlee TK (1971) Bonding mechanisms at the interface of ceramic prosthetic materials. J Biomed Mater Res 5(6):117–141
17. Ojansivu M, Vanhatupa S, Björkvik L, Häkkänen H, Kellomäki M, Autio R, Ihalainen JA, Hupa L, Miettinen S (2015) Bioactive glass ions as strong enhancers of osteogenic differentiation in human adipose stem cells. Acta Biomater 21:190–203

18. Balasubramanian P, Hupa L, Jokic B, Detsch R, Grünewald A, Boccaccini AR (2017) Angiogenic potential of boron-containing bioactive glasses: in vitro study. J Mater Sci 52(15):8785–8792
19. Vallet-Regí M, Ragel CV, Salinas AJ (2003) Glasses with medical applications. Eur J Inorg Chem 2003(6):1029–1042
20. Bellucci D, Sola A, Salvatori R, Anesi A, Chiarini L, Cannillo V (2014) Sol–gel derived bioactive glasses with low tendency to crystallize: synthesis, post-sintering bioactivity and possible application for the production of porous scaffolds. Mater Sci Eng C 43:573–586
21. Ostrowski N, Roy A, Kumta PN (2016) Magnesium phosphate cement systems for hard tissue applications: a review. ACS Biomaterials Science & Engineering 2(7):1067–1083
22. Kokubo T, Takadama H (2006) How useful is SBF in predicting in vivo bone bioactivity? Biomaterials 27(15):2907–2915
23. Bassyouni FA et al (2014) Synthesis and biological evaluation of some new triazolo [1, 5-a] quinoline derivatives as anticancer and antimicrobial agents. RSC Adv 4(46):24131–24141
24. Suzuki T, Yamamoto T, Toriyama M, Nishizawa K, Yokogawa Y, Mucalo MR, Kawamoto Y, Nagata F, Kameyama T (1997) Surface instability of calcium phosphate ceramics in tissue culture medium and the effect on adhesion and growth of anchorage-dependent animal cells. Journal of Biomedical Materials Research: An Official Journal of The Society for Biomaterials and The Japanese Society for Biomaterials 34(4):507–517
25. Ohgaki M, Kizuki T, Katsura M, Yamashita K (2001) Manipulation of selective cell adhesion and growth by surface charges of electrically polarized hydroxyapatite. Journal of Biomedical Materials Research: An Official Journal of The Society for Biomaterials, The Japanese Society for Biomaterials, and The Australian Society for Biomaterials and the Korean Society for Biomaterials 57(3):366–373
26. Teng N et al (2001) A new approach to enhancement of bone formation by electrically polarized hydroxyapatite. J Dent Res 80(10):1925–1929
27. Smith I, Baumann M, McCabe L (2004) Electrostatic interactions as a predictor for osteoblast attachment to biomaterials. Journal of Biomedical Materials Research Part A: An Official Journal of The Society for Biomaterials, The Japanese Society for Biomaterials, and The Australian Society for Biomaterials and the Korean Society for Biomaterials 70(3):436–441
28. Sarkar K, Rahaman M, Agarwal S, Bodhak S, Halder S, Nandi SK, Roy M (2020) Degradability and in vivo biocompatibility of doped magnesium phosphate bioceramic scaffolds. Mater Lett 259: 126892
29. Wang Z, Ma Y, Wei J, Chen X, Cao L, Weng W, Li Q, Guo H, Su J (2017) Effects of sintering temperature on surface morphology/microstructure, in vitro degradability, mineralization and osteoblast response to magnesium phosphate as biomedical material. Sci Rep 7(1):823
30. Farag MM, Al-Rashidy ZM, Ahmed MM (2019) In vitro drug release behavior of Ce-doped nano-bioactive glass carriers under oxidative stress. J Mater Sci Mater Med 30(2):18
31. Jia J, Zhou H, Wei J, Jiang X, Hua H, Chen F, Wei S, Shin JW, Liu C (2010) Development of magnesium calcium phosphate biocement for bone regeneration. J R Soc Interface 7(49):1171–1180